HY13897

Close-Range Photogrammetry Application to Monitor Levee Erosion in Case of Wave Overtopping

Masoumeh Ebrahimi[1], Myron van Damme, Ph.D.[2], Henk van Hemert, Ir.[3], and Sandra Soares-Frazão[4*]

1 Ph.D. Candidate, Institute of Mechanics, Materials and Civil Engineering, Université Catholique de Louvain, Place du Levant, 1 box L5.05.01 Louvain-la-Neuve 1348, Belgium. Email: masoumeh.ebrahimi@uclouvain.be. (ASCE membership grade S.M.ASCE)

2 Senior Technical Advisor, Rijkswaterstaat WVL, Griffioenlaan 2, Utrecht 3526 LA, the Netherlands. Email: myron.van.damme@rws.nl.

3 Coordinating Specialist Advisor, Rijkswaterstaat WVL, Zuiderwagenplein 2, Lelystad 8224 AD, the Netherlands. Email: henk.van.hemert@rws.nl.

4 Professor, Institute of Mechanics, Materials and Civil Engineering, Université Catholique de Louvain, Place du Levant, 1 box L5.05.01, Louvain-la-Neuve 1348, Belgium. Email: sandra.soares-frazao@uclouvain.be (*corresponding author).

Abstract

Coastal and riverine levees are prone to wave and steady-flow overtopping which can result in breaching and consequential flooding of the hinterland. Full-scale field experiments on a levee are a sound approach to understanding of the underlying physical processes without suffering from scale effects, provided that accurate and valuable data can be collected. This paper outlines how close-range photogrammetry was applied to monitor a levee’s morphological evolution continuously and intermittently during wave overtopping. High-resolution spatial topographical models were obtained from which erosion rates can be quantified. Two camera set-ups —a system of multi-stationary synchronized cameras, and a single mobile camera — were used for photo acquisition. The first configuration enables reconstruction of the target zone as a dynamic scene and reduces the photogrammetric analysis time through simultaneous processing of several frames [four-dimensional (4D) processing]. The second configuration applied the structure-from-motion

(SfM) technique using multiple overlapping photographs to obtain three-dimensional (3D) elevation models at specific moments. Both approaches resulted in high-resolution digital elevation models (DEMs) with low mean absolute errors (MAEs) on the order of magnitude of a few centimeters. Furthermore, photogrammetry proved to be highly flexible and could be applied to different types of levees with various cover layers, hydraulic loads, and meteorological conditions. [DOI: **10.1061/JHEND8.HYENG-13897**]

Practical Applications

Monitoring erosion processes due to wave overtopping of levees was achieved here using close-range photogrammetry in two series of field experiments with distinct camera setups. The experiments were conducted at 1:1 scale at the Living Lab Hedwige Prosperpolder to study the erosion processes of the levee's clay's protection layer (1-m-thick clay) on the landward-side slope subjected to loads by overtopping waves. The experiments were conducted on a levee cover in (i) its natural state, and (ii) after treating clay with lime for reinforcement. In the first series of experiments, a system of ten synchronized stationary cameras was used to capture photos. To focus on the erodibility of the natural clay cover, the 0.2-m-thick grass cover was removed over an area of 14 m^2 at three locations on the slope prior to testing. In the second series, a single camera was moved around the scene at specific time intervals. An object featuring a building was also embedded in each new slope revetment to evaluate the effects of flow around obstacles on erosion process. Both generated accurate erosion maps, with a slightly higher accuracy and ease of post-treatment for the multiple-camera setup.

Keywords: Prototype dike experimentation, Polder2C's, lime-treated clay, breaching, high-resolution 3D reconstruction.

Introduction

Deltas are often prone to continuous urban and industrial development. Earthen embankments, e.g., sea dikes and levees form the main defense of these low-lying coastal regions. Mean sea levels and the likelihood of occurrence of extreme events are both increasing due to climate change (IPCC 2022), causing for a higher return period of extreme loading conditions like wave overtopping of levees. For example, long-term observations at the mouth of the Western Scheldt estuary for 1848-1990 show a considerable increase in spring tide amplitudes and at least a 30 cm rise in sea level over this period, as well as increasing precipitations in the north of the North Sea region (Quante and Colijn 2016). Most of the North Sea region is protected by earthen levee networks which must withstand an increased probability of overtopping.

Levee breaching induced by steady overtopping (overflowing) and wave overtopping is one of the dominant causes of failure (ASCE/EWRI Task Committee on Dam/Levee Breaching 2011). During overtopping, the breach initiates due to continuous surface erosion of the crest and landward levee slope. Many research projects have been dedicated to studying breach formation and development in large scale embankment dams or levees, e.g., IMPACT (Morris et al. 2007), USDARS (Hanson et al. 2005), Sigmaplan (Peeters et al. 2015). A series of large-scale riverine levee breaching experiments were conducted at the Chiyoda experimental field flume (Shimada et al. 2009, Shimada et al. 2010, Tobita et al. 2014, and Kakinuma and Shimizu 2014). All these projects concerned fully destructive breaching experiments to investigate the general breach expansion due to frontal or longitudinal riverine overtopping.

To reinforce the flood protection system without increasing the height of levees, one possible solution is to design levees capable of withstanding higher overflowing and wave overtopping discharges. This necessitates research on the erosion resistance and strength of the levee's landward side slope and quantifying the erosion progression into the soil. Furthermore, to meet the new standards and regulations, there is a growing demand for the safety and strength assessment of levees through real-scale, partially destructive experiments (van Damme et al. 2016, Rikkert et al. 2022, Picault et al. 2022). ASCE/EWRI Task Committee on Dam/Levee Breaching (2011) emphasizes the importance and necessity of conducting large-scale and prototype experiments to accurately replicate the complex physical processes and avoid scale effects (e.g., levee material reproduction and vegetation impact) inherent in small-scale modeling. Partially destructive experiments are widely conducted in the Netherlands (van Damme et al. 2016, Koelewijn et al. 2022) and more recently in France along the Rhône River (Picault et al. 2022). The limited damage in these experiments, is easier to execute and monitor. These tests also enable a closer observation of the soil-flow interaction over a limited area, and therefore offer an advantageous way to evaluate the instantaneous strength of a protective cover layer under extreme events. Particularly during the last two decades, a large number of partially destructive full-scale experiments was conducted on real levees, investigating the behavior of landward slope under overflowing and wave overtopping conditions, or WOCs, (van der Meer et al. 2009, Steendam et al. 2012, van Damme et al. 2016, Koelewijn et al. 2022; Ponsioen et al. 2019). These field tests have been used to investigate the strength of grass-cover on the landside slope under wave overtopping conditions (van der Meer et al. 2009, Steendam et al. 2012, Steendam et al. 2013) or they have been implemented to gain more insight into the correlation between flow characteristics and the overtopping volumes (van der Meer et al. 2010, Hughes et al. 2012).

Furthermore, to upgrade levees and make them resistant to overtopping, sustainable soil-based reinforcement techniques have become popular. For instance, clay treatment by lime is being recognized more regularly as a cover reinforcement method. According to the state-of-the-art review of lime treated clay (LTC) application to earth-fill dikes (Puiatti et al. 2018), adding lime to clay enhances its resistance to erosion (Bennabi et al. 2016). Using eco-friendly additives substances such as biopolymers offer an alternative method to decrease the soil erodibility and thereby enhance the levee resistance under steady overflow and wave overtopping conditions (Ko and Kang 2018). Ideally, the effectiveness of such techniques is verified through full-scale in-situ experiments prior to widespread application.

In this context, acquisition of high-quality data during full-scale experimental campaigns through cost-effective and user-friendly measurement techniques is of the utmost importance for the development and calibration of mathematical models describing underlying physical processes (ASCE/EWRI Task Committee on Dam/Levee Breaching 2011). However, most available data on damage initiation and progression are limited to either pixel-based image analysis or pointwise ground survey measurements (van der Meer et al. 2009). In addition, there is scarce information on the erosion progression into the soil underneath the grass cover. According to Dutch regulations (van der Meer et al. 2015) the protective grass layer is considered to have failed when the damage penetrates the turf layer. However, the erosion processes in clay after failure of the grass cover need to be investigated further (D'Eliso, 2007). Despite recent advancement in field experimentation, monitoring temporal evolution of progressive levee breaching in case of steady and wave overtopping remains a challenge. Regarding fully destructive tests, Morris et al. (2007) embedded sensors into a test dike and recorded the time of their movement to monitor the breach growth; they also printed a grid on the crest and the downstream slope of the dike to allow for capturing the lateral breach enlargement above water level from video footages. Hanson et al. (2005) used a point gauge in form of a vertical rod to measure water levels and bed profiles at the centerline of the embankment during large-scale experiments. Using a combination of centerline profiles and photographic analysis, they determined the headcut location. Recently, Shimada et al. (2009), Shimada et al. (2010), and Tobita et al. (2014) developed a technique to record breach geometry evolution under the flow, using acceleration sensors placed in longitudinal and transversal sections in the levee. Lidar or terrestrial laser scanners (Herrero-Huerta et al. 2016, Bento et al. 2022) also enable initial, final, and occasionally intermittent bed level profile detection and 3D surface maps reconstruction.

Close-range photogrammetry may also be an attractive method for monitoring field-scale experiments. This is becoming increasingly popular and efficient as a nonintrusive laboratory measurement technique (Lane et al. 2001, d'Odeigne et al. 2018, Bento et al. 2022). The Structure-from-motion (SfM) technique (Snavely 2008, Westoby et al. 2012) generate high-resolution 3D models of objects or terrain for remote sensing purposes. The method has already been applied to a wide range of studies such as monitoring changes in water surfaces, river bed topography, morphology, soil and river bank erosion (e.g. Barker et al. 1997, Lane et al. 2001, Heng and Chandler 2010, Barkker and Lane 2017, d'Odeigne et al. 2018, Zhang et al. 2022). Dezert and Sigtryggsdóttir (2024) employed SfM technique to monitor the displacement of levee riprap protection layer exposed to levee constant overtopping in a small-scale setup. Rieke-Zapp and Nearing (2005) showed that high-resolution Digital Elevation Models (DEMs) with 1-mm vertical precision for an erodible surface of 16 m^2 are achievable to measure micro topographical changes. Bento et al. (2022) implemented this technique to accurately characterize the final shape of a scour hole formed in the vicinity of a bridge pier in the laboratory environment. All these studies demonstrated the capability of close-range photogrammetry in reconstructing highly accurate 3D models across a wide range of hydraulic engineering problems. However, field applications of close-range photogrammetry to continuous monitoring of erosion under less favorable weather and lightning conditions are required to further investigate the applicability of this technique.

This paper shows the capacity of close-range photogrammetry to monitor the morphological evolutions of the landward side slope of a prototype levee subjected to simulated overtopping waves. The levee slope evolution was photographed using two different camera installation set-ups during the experiments. The photogrammetric reconstruction (3D model) of the scene was carried out using Agisoft Metashape (Agisoft Metashape User Manual 2022). The main processing parameters of the software for both camera set-ups (fixed multiple-camera, single mobile camera) had been verified and optimized to obtain high-resolution accurate elevation models. The experiments were conducted in the Living Lab Hedwige-Prosperpolder (LLHPP) located near the border of Belgium and the Netherlands next to Western Scheldt River (Fig. 1). Wave overtopping tests were conducted to evaluate the erosion resistance of bare natural clay underneath the grass sod as well as a new cover constructed from innovative lime-treated clay mixtures.

This paper is organized as follows: first the in-situ setup and testing procedures are described. Then, the close-range photogrammetry application using the two different camera set-ups are presented. The performance of the technique for field-scale measurements are discussed and assessed, and finally, conclusions and perspectives of this research are provided.

In-situ Setup and Testing Procedures

The Living Lab Hedwige Prosperpolder (LLHPP) was a 6-km^2 agricultural area that was converted into a natural tidal zone as shown in Fig. 1. With the creation of a new levee, the old levees protecting the polder became redundant, offering a vast laboratory to conduct a wide range of destructive experiments on actual levees (Rikkert et al. 2021, Koelewijn et al. 2022) at different scales and to practice innovative levee emergency response strategies within the Polder2C's project. The levees in the LLHPP area consisted of a sand core protected by an approximately 1-m thick well-grassed clay layer cover (Fig. 2), and have an average steepness of 1V:2.6H. Soil investigation pits excavated next to the testing zones indicated that the clay cover layer had an average thickness of 0.8 m, with values ranging from 0.75 m near the toe and crest to 1 m in the middle of the slope. Heterogeneities within the soil profiles were observed both in-depth and along the levee slope, exhibiting variations from clay soil to silty sand containing grass roots. The median grain diameter (d_{50}) ranged from 88 to 150 µm in different soil samples taken from different depths in the cover layer (van Damme et al., unpublished Polder2Cs report, 2023). The upper part of the protective clay layer included grass and roots with crumbled soil (0.1 meter thick).

The first series of tests investigated the performance of natural clay, hereafter called bare-clay (BC) erosion tests, while the second series aimed at evaluating the resistance of three different lime-treated clay (LTC) mixtures developed to enhance the erosion resistive properties of clay. Critical flow velocities and shear stresses for erosion initiation were determined by performing tests with the Erosion Function Apparatus (EFA) for both BC and LTC soils. While critical flow velocities and shear stresses ranged from 0.4 to 0.6 m/s, and 0.6 to 1 Pa, respectively, for samples taken from BC test sections, almost no erosion was observed in case of LTC soil samples for flow velocities under 2.6 m/s. The levee stretches where BC and LTC experiments were conducted are indicated in Fig. 1. The Wave Overtopping Simulator (WOS) (van der Meer et al. 2007) was placed on the levee crest to release either Weibull distributed wave volumes or constant wave volumes.

The exact locations of all test sections were recorded using an RTK GNSS GPS tool with a precision of 1-2 cm, in RD 2008 (Netherlands/RD) - EPSG:28992 coordinate reference system (CRS). In this system, the position of each point is defined as Easting, Northing, and Elevation. The Elevation is the absolute upward elevation of each point in meters with regard to the Normaal Amsterdams Peil (NAP) which is the Amsterdam ordnance datum. As illustrated in Fig. 3, the Easting and Northing were then transferred into a conventional coordinate systems called Global (X,Y,Z), while distances along the dike slope were measured in a local system (x,y,z) located at the top left corner of the testing flumes. The xz plane is obtained by rotating the XZ plane clockwise around the Y-axis by an angle equal to the levee gradient. Thus, x-axis is aligned with the slope and is perpendicular to z-axis.

Bare-clay (BC) Erosion Tests

These tests focus on the damage initiation and progression into the top-clay layer below the grass cover. The erosion tests were repeated several times locally in this area (Koelewijn et al. 2022). Two separate 4-m wide test flumes were constructed on the landward-side slope of the levee by installing wooden lateral walls. As illustrated in Fig. 2 (a) and Fig. 3 (a), each flume was divided into a series of test sections over which a 20-cm grass cover layer was removed using a crane bucket. An example of the prepared test section is shown in Fig. 2 (b). This preparation appeared necessary after the preliminary tests showed that the grass cover itself was able to withstand the wave overtopping loads for a long time duration. The test sections were prepared and tested respectively from the toe towards the crest, to allow for three tests on the same portion of the levee, i.e., test section BC1-1 was tested before test section BC1-2 for example. Due to the supercritical wave velocities, the loads would not be affected by the erosion of the lower lying test sections, whereas the grass cover present on test section BC1-2 would prevent erosion of this while testing section BC1-1. Only shortly prior to testing the sections, the grass cover was removed. The test sections were approximately 3.5 m long, ensuring that waves would not overshoot the test sections, and that the test section would indeed constitute the weakest parts of the levee. As a result, during each test, a section of roughly 14 m^2 of clay was exposed to the waves. Sections BC2-1 and BC2-2 were prepared in a similar way. The resulting initial dike profiles for test BC1 are illustrated in Fig. 3 (b).

The clay layer was considered to have failed as soon as the erosion reached the sand core (D'Eliso 2007). This criterion is highly conservative, as erosion may occur locally, and form deep, narrow holes, without leading to an immediate failure of the levee. However, such holes constitute weak points in the levee that significantly affect its strength and ultimately lead to a full failure.

Lime-Treated Clay (LTC) Erosion Tests

To investigate the improvement in erosion resistance brought by the lime treatment, especially in the vicinity of transitions and obstacles on the levee slope (Steedman et al. 2014), the original clay cover of the levee was replaced by a lime-treated clay cover over the entire levee stretch as shown in Fig. 4 (a). This stretch was divided into three main sections (LTCB1, LTCB2, and LTCB3), each test section being constructed with a specific clay and equipped with a wooden block, representing a structure partially embedded in the levee.

Three types of clay were tested and used in accordance with the Dutch Dike Construction Manual (Halter et al. 2018). To properly estimate the erosion resistance of clay, the Dutch Dike regulations use Atterberg limits, including the A-line from the plasticity graph of Casagrande (Halter et al. 2018) and classify the original soils into three categories. Fig. 5 displays that the three clay soils (A, B, C) are within the limits of erosion-resistant clay for levee revetment utilization. Meanwhile, clay types A and B are located close to the moderately erosion-resistant clay category limits and less favorable for dike revetment. Hence, soils type A and B are referred to as lesser quality clays, and clay type C as good quality clay in this paper. Clay type C was transported to and stored in the LLHPP while clays A and B originated from the LLHPP. These clays can turn into very resistant material once treated with lime. The lime content of treated soil is 5 % of the dry soil weight for clay type C, and 4 % for both clay soils type A and B according to Stoutjesdijk (2022). The amount of required lime depends on a soil property known as Lime Fixation Point (LFP) slightly above which (1 to 2%) the pozzolanic reaction occurs and leads to the soil strengthening. The LFP can be determined from the Atterberg limits tests on clay soils mixed with varying amounts of lime (Hilt and Davidson 1960). The plastic limit remains almost constant slightly above the LFP in all clay soils. The agglomeration and the binding of the particles to each other, under the action of lime, increase the shear stress required to tear off the soil particles (Bennabi et. al. 2016). The EFA tests on the treated soils (types A, B, C) indicated a significantly increase in erosion resistance (Stoutjesdijk 2022).

The clay soil types A, B, and C are used respectively to reconstruct the levee cover including three 4 m wide flumes in which a scaled-down building (wooden box) was constructed in the middle of each flume named respectively as LTCB1-A, LTCB2-B and LTCB3-C (see Fig. 4 (a)). Apart from the variability in soil properties between test sections, a stronger compacter was used to compact the soil around the obstacle in test flumes LTCB2-B and LTCB3-C than in flume LTCB1-A.

Preparation of the levee revetment started with removal of the existing protective layer. To prevent geotechnical instability of the new cover, the grass cover and the upper clay soil layer were removed in a staircase shape (width 1 m × height 0.4 m) as depicted in Fig. 6 (a). The new levee cover, therefore, was constructed on this staircase profile following the same form. The final cover layer had a variable thickness changing between 0.4 to 0.75 m along the slope after cutting the final slope as shown in Fig. 6 (b) (Stoutjesdijk 2022). Each layer was compacted horizontally and in stretches parallel to the crest line with a Padfoot or Sheepsfoot drum compactor machine. The Proctor Compaction Test parameters after lime-treatment (4%) were determined to be ω_{optimum} = 27 % and $\gamma_d^{max} = 15$ kN/m^3; however, this was not strictly controlled during construction. The final slope of 1:2.6 was created by cutting and removing excess material. Despite that, remnants of the compactor and soil layers are still visible on the prepared test flumes, as can be recognized in Fig. 4 (a).

Wave Overtopping Load Conditions

Waves were generated in a controlled way using the WOS located on the levee crest (Fig. 7 (a)). The simulator allowed for predetermined volumes of water to be released (see Fig. 7 (b)) as a series of pulses, imitating natural wave overtopping events. The volume of water in the simulator was measured with a pressure transducer that caused valves to open automatically when the prescribed volume was reached. The operational details of the simulator are explained by van der Meer et al. (2007).

The WOS can generate periodic waves with regular or irregular (i.e., more realistic) patterns, as illustrated in Fig. 8. Irregular waves (Fig. 8 (a)) were released over a fixed period with random volumes according to a Weibull distribution, corresponding to a prescribed average discharge. These waves are defined by the significant wave height and peak period of incident waves that can overtop the levee. Here, the tests are generally named with an acronym that includes the mean discharge q in L/s/m or m^3/s/m and the significant wave height H_s (van der Meer et al. 2007) e.g., a test called 0.5m60lsm corresponds to an average discharge of 60 L/s/m and a significant wave height of 0.5m. Regular waves (Fig. 8 (b)) consisted of a combination of 10 or 20 waves with constant volumes over a time interval, to produce a prescribed average discharge. During the experiments small wave volumes were omitted to reduce the experimental duration. For the regular waves, a descending or increasing total volume trend was imposed during the tests, with a stepped-form pattern as illustrated in Fig. 9 (a), (b), and (c).

Fig. 9 (a), (b), (c), and (d) illustrate the regular and irregular waves used to simulate wave overtopping storms of approximately 2 hours at BC test sections. The BC1-1, BC1-2 and BC1-3 sections were tested under a series of regular wave groups of similar wave volumes per group.

An increasing trend was applied for BC1-1 that was then adjusted for the other tests BC1-2 and BC1-3, located higher on the levee, i.e., closer to the crest. At these higher sections, the experiments began with high overtopping volumes, followed by an intermittent stepwise decrease in overtopping volumes and an instantaneous increase at the end. This modification of the wave pattern was done to examine the soil reaction under different scenarios and to identify the dependence of the erosion progression on the release order of the wave volumes. The second series of tests, performed on flume BC2, concerned more realistic wave overtopping conditions with irregular waves corresponding to river (BC2-1) and coastal wave conditions (BC2-2), as shown in Fig. 9 (d) and summarized in Table 1. Both the height and peak period of coastal waves are larger than those of river waves for the same mean discharges. As a result, the number of waves with higher volumes is significantly larger for coastal dikes (van der Meer et al. 2010), whereas the total number of waves is smaller. The average discharge of storm events simulated at test sections BC2-1 and BC2-2 are 0.06 m^3/s and 0.05 m^3/s, and wave significant heights of 0.5 and 1 m, respectively (Table 1).

The LTCB experiments, summarized in Table 1, comprised a series of overtopping events, with irregular waves. The overtopping storm lasted nearly 9 hours of continuous testing at LTCB1-A (halted at the beginning of 2m50lsm due to obstacle failure), and 11 hours at both LTCB2-B and LTCB3-C. This duration is typically sufficient to simulate an entire wave overtopping event during a design storm and consequently produce the maximum erosive load (EurOtop 2018). For the simulated storm events executed at LTCB sections the mean wave overtopping discharge was incrementally increased in a step wise manner (Fig. 10).

Photogrammetry Measurement Technique: Application and Verification

Photographs of the different tests were recorded to apply the photogrammetry technique, i.e., 3D geometry reconstruction from multiple overlapping images based on scene triangulation principle, using the commercial software Agisoft Metashape. The principles of close-range photogrammetry and recent advancements in this field i.e., 'Structure-from-Motion' (SfM) are discussed by Lane (2001), Snavely (2008) and Westoby et al. (2012) . In contrary to traditional photogrammetry, the SfM method does not require the exact position of cameras or the 3D location of some known points to resolve the 3D structure. However, to represent the results in a global coordinate system, Ground Control Points (GCP) with known coordinates were positioned around the scene and visible on the images (see Fig. 2). The photogrammetric processing (Agisoft Metashape User Manual 2022) is summarized in Fig. 11 as an example taken from the BC tests: after loading raw images (Fig. 11 (a)), these were orthorectified and aligned using the identification of the GCPs (Fig. 11 (b)); a dense point cloud was produced (Fig. 11 (c)). Finally, the georeferenced Digital Elevation Model (DEM) was constructed on a regular grid (Fig. 11 (d)) and corresponding orthophotos were created (Fig. 11 (e)).

The process was robust in reproducing constant and repeatable DEMs with low standard deviations (also shown by Zhang et al. 2022, Kingsland 2020, Bento et al. 2022, Dezert and Sigtryggsdóttir 2024). During the experiments, GoPro HERO9 cameras (GoPro, Inc, San Mateo, California, USA) were used in wide-angle lens mode to increases the field of view on each picture. This enabled a good overlap of images, which was a key condition for an accurate analysis, but it also resulted in highly distorted images (Fig. 11 (a)), which required correction to obtain an orthorectified image. This correction is automatically applied during photo alignment, provided that the proper camera distortion type (Frame, Fisheye, and Spherical) is selected in the Camera Calibration step. The software uses the corresponding camera model (here, Fisheye) and applies the appropriate distortion model to orthorectify the photos. The resulting DEMs have a spatial resolution of 0.002 m in the *x*- and *y*-directions.

In this study, the method was applied in two different ways: (i) using a set of 10 cameras located at fixed positions for the BC tests, and (ii) using one single camera moved around the scene for the LTCB tests, as in the original Structure from Motion (SfM) technique developed by Westoby et al. (2012). To apply the photogrammetry technique from a set of images, it is necessary to have a sufficient overlap between images including at least one GCP. However, identifying at least three common well-distributed GCPs, which include two opposite corners of the scene on each image, allows to achieve the highest accuracy. To determine the optimal number of cameras or photos in each set-up, the following procedure was applied: using one single camera, photos were taken from various angles and locations around the scene, followed by the reconstruction of an initial 3D model in the software. The optimal number of cameras was determined based on the quality of the resulting 3D models. In the present case, it was found that 10 cameras, located as illustrated in Fig. 12, provide an optimal 3D reconstruction of the scene. The camera set-ups corresponding to each type of application are presented in the next sections, followed by a discussion of the resulting accuracies. Table 2 summarizes all erosion test types and the corresponding image acquisition method at each test section.

Multiple fixed cameras supported by a rigid frame.

In order to monitor the BC experiments in a continuous way, a system of multi-stationary synchronized cameras was employed. Photogrammetry could be then employed at any moments between wave groups to quantify morphological changes. In case of irregular waves with arbitrary volumes, the recognition of interesting moments was difficult prior to the experiments and a complete set of photos covering the entire experimentation facilitated the choice of interesting moments to be analyzed. Furthermore, the autonomy in photo acquisition led to minimum interruption of the tests and field works. The bare-clay test sections (BC1 and BC2) were monitored by means of 10 GoPro HERO9 cameras that were mounted on a mobile rigid frame illustrated in Fig. 12. Six of the ten cameras were installed on a frame spanning across the flume, while the remaining four were positioned on lateral columns (Ebrahimi et al. 2022). The position and angle of view of the cameras ensured maximum overlap and a complete coverage of the monitored area. The precise location of each camera was not important for the photogrammetric analysis provided that GCPs were installed and that their three-dimensional coordinates were known precisely. As can be seen in Fig. 12, the GCPs were installed around the test section perimeters vertically and horizontally. The coordinates of the GCPs were measured via an RTK GNSS GPS system.

The cameras were configured to take photos in time-lapse mode with a 1-second interval, capturing the test section continuously during the experiments. Sets of five cameras were synchronized with a remote control, allowing for simultaneous cameras manipulation. The cameras have a resolution of 5184×3888 in time-lapse mode and a focal length of 3 mm.

After each series of waves corresponding to a prescribed volume of water (e.g., Fig. 9), an interruption of a few minutes was imposed. This allowed the test section to partially dry out to minimize the adverse effects of measuring the water-level instead of the bed elevation. During these interruptions, pictures of the scene were taken by the 10 cameras and manual measurements of a series of arbitrary points were performed. Coordinates of these random points were recorded over the testing section providing accurate checkpoint data for assessing the accuracy of the photogrammetry technique.

The software processed several batches of photos per camera i.e., several frames in parallel, in a multi-camera setup, to reconstruct a dynamic scene of the target zone at different time moments. This feature, called 4D processing in the software, highly accelerated the photogrammetry processing but was limited to statically mounted synchronized cameras. The processing parameters introduced in Metashape and the resultant model features are outlined in Table 3. The Key and Tie point limits for multicamera system were determined by trial and error to achieve a high number of sparse points in the study region. These parameters were maintained at their default values in the software for the mobile camera set-up (SfM).

The accuracy of the photogrammetric measurements was evaluated by comparing them to the manual measurements conducted using the RTK system. Fig. 13 (a) presents the comparison between the two methods throughout the wave overtopping experiments at BC2-2 test section. The results indicate a good correspondence between two methods, with a Mean Absolute Error (MAE) of 0.04 m at this section. Overall, the photogrammetry tends to underestimate the levee erosion by overestimating the elevations. This discrepancy was attributed to the estimation of lens and exterior orientation parameters using SfM methods, which introduces an inherent systematic error in the resulting point clouds (Bakker and Lane 2017). Also, some scattered points were observed towards the downstream end of the test section (around z = 4.6 m). This inaccuracy, on one hand, was caused by water trapped into the erosion pits: in this case, the water surface is identified by the photogrammetry technique instead of actual bed elevation. On the other hand, the inaccuracy was caused by dark shadows cast on a sunny day. Fig. 13 (b) shows such zones where water was stuck in the erosion pits, primarily located at the lowest extremity of the test section. One solution would have been to leave enough time between the wave pulses to allow most of the water to naturally drain away, but the time scheduling of the experiments limited the drainage effectiveness. Therefore, it was attempted to select the photos with a minimum of residual water present in the eroded area. For the measurement of the final state, little water remaining in the erosion pits was pumped out.

The technique was applied under various meteorological conditions, including cloudy, rainy, and sunny weathers in the field. Cloudy weather proved to be the most favorable condition for obtaining high-resolution sharp photos. While light reflection, contrast, or shadows may influence the quality of photos during sunny days, they do not diminish the applicability of this technique.

One mobile camera

For the lime-treated clay experiments, continuous filming of the test section was not a priority, as the soil was less erodible. Consequently, the number of monitoring intervals during the experiments was reduced. Moreover, the tests could be interrupted over a longer duration between wave pulses, allowing sufficient time for photography. Photos acquisitions were conducted every 30 minutes using just one GoPro camera attached to a monopod. The camera was moved around the entire test flume, capturing a higher number of photos close to the obstacle. The region of interest for these tests was the area around the obstacle as indicated on Fig. 4 (a). The GCPs were densely placed over a certain radius around the obstacle (Fig. 14 (a)), where flow concentration was expected to result in significant erosion. On average, 100 photos were captured to encompass the entire flume, of which 80 to 90 photos were successfully aligned. The software finds and matches common points in overlapping regions of the images, while the GCPs are essential to locate them geospatially, and to scale the 3D model. The resulting orthophoto image is shown in Fig. 14 (b).

Manual measurements were taken to evaluate the accuracy of the method, as illustrated in Fig. 14 (c) for the tests at LTCB1-A. In this section, the accuracy was found to be of the order of 0.05 m (MAE) which is similar to the one obtained using the fixed multi-camera method, even for the furthest points situated near the crest and toe of the levee. Except for two points encircled in Fig. 14 (c), all other points closely align with the inclined line representing the equality of measurement and calculations. The points with maximum errors are located next to the obstacle in a deep narrow trench, which was difficult to reach with the camera. As in the previous case, the elevations are generally overestimated by the photogrammetry technique.

The comparison between Fig. 13 (a), derived for a multicamera system, and Fig. 14 (c), resulting from a single mobile camera setup, suggests that increasing the number of images does not automatically result in more accurate DEMs. The key factors influencing the accuracy are the overlap and configuration of the images, as demonstrated by Bakker and Lane (2017).

Results from the photogrammetry measurements

Table 4 summarizes the photogrammetry analysis performed throughout BC experiments, after different number of waves indicated in Fig. 9 (a), (b), and (c) for BC1 experiments. For LTCB tests, the moments at which the analysis was conducted for each storm condition is indicated in Fig. 10.

BC experiments

The observations indicate that the clay cover failure was mostly a local phenomenon whereby a deep scour hole formed, which either developed into a headcut moving upwards or remained locally restricted. In fact, as soon as a relatively weak point in the prepared soil became affected, the erosion concentrated around this point. This is illustrated in Fig. 15 showing the final state of bare-clay tests and the bed changes (ΔZ) at the end of experiment. In the BC1-1, BC2-1 and BC2-2 sections, the erosion concentrated at some spots that developed more rapidly and got dominant afterward. In BC2-1 test, the erosion grew upward while it remained more restricted in the BC1-1 and BC2-2 sections. This evolution is depicted in Fig. 16 for BC2-2, which showed that the erosion was not evenly distributed along the width, and that a localized erosion pit formed. This observation is in accordance with the large-scale experiments conducted by Hanson et al. (2005) emphasizing the development of an initial scour hole into a steep headcut migrating upstream from the test section. Another interesting point is the slope steepening of the levee side at the end of tests. Regarding test BC1-3, located close to the levee crest and thus close to the WOS, the erosion depth was observed to be more uniformly distributed, and on average larger than for the other test sections located further downstream. This is due to the strong increase in wave volumes at the beginning and end of the test (Fig. 9 (c)). Interestingly, even after generating waves at maximum capacity of the simulator i.e., 3000 l/m, the erosion did not penetrate as deep as at the lowest sections BC1-2 and BC1-1. This is explained by the way how waves attack the slope i.e., normal, or tangential. The dominant load direction close to the crest is normal to the levee slope and it progressively turns into tangential with high shear stresses as the wave travels towards the levee toe. At those location where the wave front changes direction due to a local change in levee slope, the normal stresses increase significantly again (see Fig. 17).

A detailed examination of the influence of test location on soil damage magnitude revealed that higher flow velocities near the toe, combined with the shape of the test section, led to stronger wave jumps at the lowest test sections, as illustrated in Fig. 17 (a) and (b). This is confirmed when comparing the magnitude of soil loss at the lower (BC1-1 and BC2-1) and middle (BC1-2 and BC2-2) sections. Although stronger overtopping storm events are simulated at the BC1-2 and BC2-2 sections, which are located at the middle of the levee slope, a lower maximum and average erosion depths were observed at these sections compared to BC1-1 and

BC2-1 (located at the lowest part of the levee). This implies that the loads exerted by the waves on the clay were significantly reduced at the transitory area i.e., halfway down the slope from the crest inner line.

The evolution of longitudinal profiles representing average levee elevation across the flume (averaged over the transversal direction, i.e., *y*-axis), and the maximum bed level changes along the *x*-axis where a scour hole was formed at BC1-1 test section are shown in Fig. 18 and Fig. 19 (a). While the temporal evolution of the average profiles shows a smooth evolution of the bed level along the slope, the maximum eroded profiles present significantly higher and variable erosion depths (Fig. 19 (b)).

Table 5 outlines the total mass loss as well as the maximum and average erosion depth per test section. The results indicate that the maximum erosion depth is greater for the irregular wave tests (BC2) compared to the regular wave tests (BC1), despite the average overtopping discharge being lower for BC2 (Table 5). This implies that the number of waves and total overtopping volumes (which were significantly higher in the BC2 sections compared to the BC1 sections) play a more critical role in governing erosion progression than the average overtopping discharge.

LTCB experiments

In all three test flumes, the remaining loose and less compacted soil were washed away after 30 minutes (WOC1), corresponding to Fig. 20. (b) at LTCB1-A. The morphological evolution of the levee slope at this section is illustrated in Fig. 20. After this transitory stage, the levee slope changes remained limited. Besides, morphological changes over the target study zone after 1m190lsm (WOC4 in Fig. 20 (c)) were negligible in all LTCB experiments, and this 1m190lsm was selected as the final state of soil.

The erosion initiated along a series of lines that were the footprints of the compactor. Then, the erosion concentrated where the flume width was limited by the installation of the wooden box, particularly against the obstacle parallel to the flow. As previously mentioned, the protection layer of the levee at LTCB1-A was reconstructed from lesser quality clay type A treated with lime, and using a smaller compactor around the obstacle than that of LTCB2-B (of a similar property to clay A) and LTCB3-C. The dominant form of erosion of clay at LTCB1-A was the formation of a narrow deep trench in the vicinity of the obstacle and next to the downstream corner (Fig. 20 (c) and Fig. 21 (a)). At the beginning of the 2m50lsm test, the obstacle was even torn from the soil terminating the experiments earlier than programmed.

Fig. 21 (b) and (c) demonstrate that the use of a powerful compactor around the obstacle at LTCB2-B and LTCB3-C hardly allowed for any erosion around it. All tests generally exibited erosion in a stairstep form. However, the erosion patterns differs across the target study area for all LTCB flumes as shown in Fig. 21 (a), (b), and (c). While less erosion occurred over the target study zone at LTCB3-C, steep steps or sharp cliffs were formed at this area and on the opposite side of the obstacle in case of LTCB2-B. Both clay types B and C highly eroded in stair-step patterns as shown in Fig. 22 at higher and lower extremities of the levee slope dictated by the construction procedure. It appears that the vertical discontinuities between adjacent layers (see Fig. 6), dictated by the construction protocol, accelerated the erosion and triggered more erosion at the layer situated at the lower side. where the soil was less compacted during construction. This is also where the soil was compacted less during construction and hence was eroded faster (indicated area on Fig. 6) leading to formation of a series of stair step cascades in clay layer.

The average and maximum erosion depths of all LTCB sections are given in Table 5. Despite a larger maximum erosion depth next to the obstacle at LTCB1-A, overall, it has a better performance than the LTCB2-B and LTCB3-C in terms of total mass loss over the target zone. It was observed that the maximum erosion depth was less for LTCB3-C than for the other test sections. One possible explanation is that the heavier compaction close to the obstacle at LTCB2-B and LTCB3-C had an adverse influence on the overall morphological evolution, transferring erosion to other regions of the slope. LTCB2-B experienced a substantially higher soil loss, and with a maximum erosion depth close to that of the LTCB1-A, had the worst performance between all test flumes. Therefore, the construction procedure had an important impact on the erodibility of the materials. Less compacted materials were removed more easily from the levee at the beginning by the low overtopping waves and therefore lead to significant erosion at the beginning.

Nevertheless, LTC soil mixtures proved to be promising for levee revetments as they are eroded very little after a relatively enormous total wave overtopping volume in comparison to BC test sections.

Conclusion

This paper has outlined the applicability of the close-range photogrammetry for in-situ levee erosion measurements through high-resolution spatial data (DEM) production. Two series of wave overtopping experiments were conducted in the LLHPP next to Scheldt River to assess the in-situ resistance of the clay covers of the levee exposed to different wave overtopping storm events. The morphological changes and soil loss were monitored and quantified using photogrammetry technique. The accuracy of the technique was assessed by comparing the resulted DEM models to manual measurements of random points over the test sections using the RTK GNSS GPS tool. It was found that the photogrammetry technique slightly overestimated the bed elevation, with a mean average error (MAE) of a few centimeters, including the adverse effects due to water presence in the section. No significant differences in accuracy were observed between the multiple-camera or single-camera setups since both provided enough photographs for accurate 3D reconstruction of test sections. The main source of error was found to be due to the presence of water remaining in the erosion pits, preventing the detection of the actual bed elevation.

The photogrammetry technique is, however, considered to be a valuable method to obtain relatively accurate results over an entire field in quite short times. The technique can be applied to similar levee problems such as levee overflowing if intermediate flow interruptions are feasible, allowing cameras to capture the soil level instead of the water surface. It can also be used to measure erosion differences due to variations in levee material, top protection (grass or artificial cover) or spatial scale. The flexibility of the method, minimal field work requirement, and its independence from meteorological conditions make it highly favorable. Still, one limitation is the required degree of precision to meet the expectations, as a general overestimation of the elevation was observed. Therefore, a preliminary analysis of the accuracy of the generated model in test conditions using alternative methods is recommended to assess the case-specific accuracy.

The wave overtopping impact on the levee bare clay (BC) cover was mainly the formation of scour holes regardless of the waves overtopping storm events patterns. The LTCB tests were conducted to examine the increase in erosion resistance levee cover layer constructed from three different clay soils treated by lime, serving as a levee reinforcement alternative. These soils had shown an excellent performance in the vicinity of the obstacle embedded halfway down the slope. However, a good soil compaction is essential to provide soil-structure integrity. Lime treatment of clay proved to be an excellent reinforcement method for turning clay into very high-resistant soil. Nevertheless, utmost attention should be given to the construction and curing of treated clay since they can highly influence the whole erosion procedure. Furthermore, a long-term monitoring of these clay mixtures is essential to evaluate how the erosion resistance of the LTCB evolve over time.

The influence of the degree of compaction on soil erodibility and the influence of the wave overtopping regime on the erosion rates should be investigated further. For the BC experiments, erosion may be primarily driven by the total wave overtopping volume, regardless of the type of wave. The correlation between the soil loss and wave overtopping volumes should be further investigated for the presented test sites and other test cases. Further analysis may enable the translation of the present research outcomes to other levees in terms of erosion rate and failure time. Additionally, the comparison between soil erodibilities at different scales (i.e., EFA and prototype results) may lead to a better understanding of the potential links between different scale tests and eventually more accurate predictions of erosion rate based on the laboratory experiments. Finally, the spatial and temporal variations in soil erodibility can be studied further by analyzing the variability in hydraulic loads, like the bed shear stress, along the slope as a function of an overtopping wave. However, this investigation requires numerical simulations, which will be conducted in the future.

Data Availability Statement

DEMs models, obtained from Agiosoft Metashape, used during this study are available on UCLouvain repository Dataverse (https://doi.org/10.14428/DVN/IW7BTM) and on Polder2C's website (https://polder2csknowledge.smartdata2030.com/public_activities/).

Acknowledgments

This research was funded via the Dutch High Water Protection Programme-Knowledge and Innovation Agenda, through the regional water authority of Limburg, the Flood Defences Knowledge Programme of the Dutch Ministry of Infrastructure and Water Management and the Interreg 2Seas programme 2014-2020 co-funded by the European Regional Development Fund under subsidy contract No [2S07-023]. Lhoist Ltd. contributed by providing the lime treated clay soils and constructing the test sections, coordinated by Roman Dobbe and Federica Bertola. The authors would like to thank André Koelewijn and Theo Stoutjesdijk who supervised, respectively, the bare-clay and lime-treated clay experiments. Many thanks to Chris Wauben and Lydia Heida from Infram-Hydren Co. who manipulated the wave overtopping simulator and did the RTK measurements. Authors want to express their gratitude to Pierre Mertens de Wilmar from LEMSC (Laboratory Mechanical Testing, Structures and Civil Engineering) of UCLouvain for his efforts during preparation of camera set-ups for photo acquisition. The authors acknowledge the three anonymous reviewers and the associate editor for their valuable comments and recommendations during the reviewing process that contributed to a stronger manuscript.

References

ASCE/Environment and Water Resources Institute (EWRI) Task Committee on Dam/Levee Breaching. 2011. “Earthen embankment breaching.” *J. Hydraul. Eng.* 137 (12): 1549–1564. https://doi.org/10.1061/(ASCE)HY.1943-7900.0000498.

Bakker, M., and S. N. Lane. 2017. “Archival photogrammetric analysis of river–floodplain systems using Structure from Motion (SfM) methods.” *Earth Surf. Process. Landf.*, 42 (8): 1274–1286. https://doi.org/10.1002/esp.4085.

Barker, R., L. Dixon, and J. Hooke. 1997. “Use of terrestrial photogrammetry for monitoring and measuring bank erosion.” *Earth Surf. Process. Landf.* 22 (13): 1217–1227. https://doi.org/10.1002/(SICI)1096-9837(199724)22:13<1217::AID-ESP819>3.0.CO;2-U.

Bennabi, A., G. Herrier, and D. Lesueur. 2016. “Lime treated soil erodibility investigated by EFA erosion testing.” *In Proc. 8th Int. Conf. on Scour and Erosion (ICSE)*, 12–15. London: Taylor and Francis.

Bento, A. M., L. Couto, T. Viseu, and J. P. Pêgo. 2022. “Image-based techniques for the advanced characterization of scour around bridge piers in laboratory.” *J. Hydraul. Eng.* 148 (6): 06022004. doi:10.1061/(ASCE)HY.1943-7900.0001981.

Carrivick, J. L., and M. W. Smith. 2019. “Fluvial and aquatic applications of Structure from Motion photogrammetry and unmanned aerial vehicle/drone technology.” *WIREs: Water.*, 6(1): e1328. https://doi.org/10.1002/wat2.1328.

Dezert, T., and F.G. Sigtryggsdóttir. 2024. ‘3D displacement and axial load of placed riprap supported at the toe: Use of structure from Motion’, *J. Hydraul. Eng.* 150(1). https://doi.org/10.1061/JHEND8.HYENG-13599.

D'Eliso, C. 2007. “Breaching of sea dikes initiated by wave overtopping: A tiered and modular modelling approach.” PhD thesis, Faculty of Architecture, Civil Engineering and Environmental Sciences TU Braunschweig, Univ., and Florence, Univ. https://doi.org/10.24355/dbbs.084-200708270200-0.

d'Odeigne, O. C., F. Franzini, G. C. M. D. Rosa, N. Janssens, and S. Soares-Frazão. 2018. "Measurement of the free-surface elevation for flows in complex topography using photogrammetry." *SimHydro*: *Advances in Hydroinformatics*. 145–156. Springer, Singapore.

Ebrahimi, M., M. van Damme, and S. Soares-Frazão. 2022. "Photogrammetry measurements of wave overtopping erosion on a seashore dike." *In Proc., 11th Int. River flow Conf.* London: Taylor and Francis.

Halter, W., I. Groenouwe, M. Tonneijck, and K. d'Angremond. 2018. "Handboek dijkenbouw: uitvoering versterking en nieuwbouw". Utrecht, Netherland: Hoogwaterbeschermingsprogramma.

Hanson, G. J., K. R. Cook, and S. L. Hunt. 2005. "Physical modeling of overtopping erosion and breach formation of cohesive embankments." *Trans. ASAE/ASABE*., 48(5): 1783–1794. https://doi.org/10.13031/2013.20012.

Heng, B. C. P., J. H. Chandler, and A. Armstrong. 2010. "Applying close range digital photogrammetry in soil erosion studies." *Photogramm. Rec.,* 25 (131): 240–265. https://doi.org/10.1111/j.1477-9730.2010.00584.x.

Herrero-Huertaa, M., R. Lindenbergh, L. Ponsioen, and M. van Damme. 2016. "Morphological changes along a dike landside slope sampled by 4D high resolution terrestrial laser scanning.*" In Proc., 23rd ISPRS Congress*, 227–232. Hannover, Germany: International Archives of the Photogrammetry, Remote Sensing and Spatial Information Sciences. https://doi.org/10.5194/isprs-archives-XLI-B3-227-2016.

Hilt, G. H., and D. T. Davidson. 1960. *Lime fixation in clayey soils*, 20–32. Washington, DC: Highway Research Board Bulletin.

Hughes, S., C. Thornton, J. van der Meer, and B. Scholl. 2012. "Improvements in describing wave overtopping processes." In *Proc., Coast. Eng.,* 1(33): 35. https://doi.org/10.9753/icce.v33.waves.35.

Intergovernmental Panel on Climate Change (IPCC). 2023. "Climate Change 2022 - Impacts, Adaptation, and Vulnerability." *Working Group II Contribution to the Sixth Assessment Report* *of the Intergovernmental Panel on Climate Change*. Cambridge University Press. https://doi.org/10.1017/9781009325844.

Kakinuma, T., and Y. Shimizu. 2014. "Large-scale experiment and numerical modeling of a riverine levee breach." *J. Hydraul. Eng.* 140 (9), 4014039–1.

Kingsland, K. 2020. "Comparative analysis of digital photogrammetry software for cultural heritage." *Digit. Appl. Archaeol. Cult. Heritage*., 20: e00157 https://doi.org/10.1016/j.daach.2020.e00157.

Koelewijn, A. R., S. J. H. Rikkert, P. Peeters, D. Depreiter, M. van Damme, and W. Zomer. 2022. "Overflow tests on grass-covered embankments at the Living Lab Hedwige-Prosperpolder: an overview." *Water*., 14: 2859. https://doi.org/10.3390/w14182859.

Ko, D., and J. Kang. 2018. "Experimental studies on the stability assessment of a levee using reinforced soil based on a biopolymer." *Water*. 10 (8):1059. https://doi.org/10.3390/w10081059.

Lane, S. N., J. H. Chandler, and K. Porfiri. 2001. "Monitoring river channel and flume surfaces with digital photogrammetry." *J. Hydraul. Eng.* 127: 871–877.

Agisoft L.L.C. 2022. "Agisoft Metashape user manual: Professional edition". Version 1.8. Agisoft LLC: St. Petersburg, Russia. https://www.agisoft.com/pdf .

Morris, M., M. Hassan, and K. A. Vaskinn. 2007. "Breach formation: Field test and laboratory experiments." *J. Hydraul. Res*., 45(1): 9–17. doi.org/10.1080/00221686.2007.9521828.

Peeters, P., G. Zhao, L. De Vos, and P. J. Visser. 2014. "Large-scale dike breaching experiments at Lillo in Belgium." *In Proc., 7th Int. Conf. on Scour and Erosion Y ICSE*. London: Taylor and Francis.

Picault C., F. Campette, S. Bonelli, S. Nicaise, N. Chaouch, F. Byron, Y. Grémeaux, A. Doghmane, M. Garoui, J. Herbeck, and F. Golay. 2022. "Field testing of the overflow erosion of Rhone river levees." *In 4th Int Seminar on Dam Protections against Overtopping*., 1-13. Madrid, Spain. https://hal.inrae.fr/hal-03924594.

Ponsioen, L., M. van Damme, B. Hofland, and P. Peeters. 2019. “Relating grass failure on the landside slope to wave overtopping induced excess normal stresses.” *Coast. Eng.*, 148: 49–56. http://dx.doi.org/10.1016/j.coastaleng.2018.12.009.

Puiatti, D., G. Herrier, N. Nerincx, S. Bonelli, and J. J. Fry. 2018. “The use of lime treated soils in water retaining structures.” In *IV Int. S* of *Earthworks in Europe*. Madrid, Spain.

Quante, M., and F. Colijn. 2016. “North Sea region climate change assessment.” *Nature*. Springer Cham. 528. https://doi.org/10.1007/978-3-319-39745-0.

Rieke-Zapp, D. H., and M. A. Nearing. 2005. “Digital close range photogrammetry for measurement of soil erosion.” *Photogramm. Rec*. 20 (109): 69–87. https://doi.org/10.1111/j.1477-9730.2005.00305.x.

Rikkert, S. J. H., C. Alleon, I. Khaldi, S. Shaiek, K. Verelst, M. Ebrahimi, F. Soares-Frazão, S. Kaidi, H. Smaoui, and P. Sergent .2021. “How strong are our levees? Hydraulic analysis based on Polder2c’s project in situ testing.” In *Proc. SimHydro*. Singapore: Springer.

Shimada, T., Y. Watanabe, H. Yokoyama, and T. Tsuji. 2009. “An experiment on overflow-induced cross-levee breach at the Chiyoda Experimental Channel.” *River, coastal and estuarine morphodynamics*. 475-481. Boca Raton, FL: Balkeme CRC Press.

Shimada, T., Y. Hirai, and T. Tsuji. 2010. “Levee breach experiment by overflow at the Chiyoda experimental channel.” In *Proc. 9th Int. Conf. on Hydro-Science and Engineering (ICHE 2010), IIT Madras, Chennai, India.* https://hdl.handle.net/20.500.11970/109830.

Snavely, K. N. 2008. “Scene Reconstruction and Visualization from Internet Photo Collections.” Doctoral thesis, Dept. of Computer Science and Engineering, Univ. of Washington.

Steendam, G. J., P. Peeters, J. van der Meer, K. van Doorslaer, and K. Trouw. 2013. “Destructive wave overtopping tests on Flemish dikes.” *Coastal Structures 2011* (In 2 volumes). 179–190. Singapore: World Scientific Publishing. https://doi.org/10.1142/9789814412216_0016.

Steendam, G. J., A. van Hoven, J. W. van der Meer, and G. Hoffmans. 2014. “Wave overtopping simulator tests on transitions and obstacles at grass-covered slopes of dikes.” *In Proc., ICCE. Reston, VA: ASCE.* 1 (34): 79. http://dx.doi.org/10.9753/icce.v34.structures.79.

Steendam, G. J., Y. Provoost, and J. van der Meer. 2012. “Destructive wave overtopping and wave run-up tests on grass covered slopes of real dikes.” *ASCE, Proc. ICCE.,* Santander, Spain. https://doi.org/10.9753/icce.v33.structures.64.

Stoutjesdijk, T. 2022. “Overtopping tests on lime treated clay in the Hedwigepolder.” Deltares report. Delft, Netherlands: Deltares.

Tobita, D., T. Kakinuma, H. Yokoyama, and A. Takeda. 2014. “Quantification of levee breach volume based on levee breach at the chiyoda experimental flume.” *J. JSCE*, 2 (1): 136-143. https://doi.org/10.2208/journalofjsce.2.1_136.

van Damme, M., L. Ponsioen, M. Herrero, and P. Peeters. 2016. “Comparing overflow and wave-overtopping induced breach initiation mechanisms in an embankment breach experiment.” *Flood Risk*., 7 (03004). https://doi.org/10.1051/e3sconf/20160703004.

van der Meer, J., P. Bernardini, W. Snijders, and E. Regeling. 2007. “The wave overtopping simulator”. *Coast. Eng.*, 5: 4654–4666.

van der Meer, J., R. Schrijver, B. Hardeman, A. van Hoven, H. Verheij, and G. J. Steendam. 2009. “Guidance on erosion resistance of inner slopes of dikes from three years of testing with the Wave Overtopping Simulator.” In *Proc*., *9th Annual Int*. *Coasts, marine structures, and breakwaters: Adapting to change*. *Conf.* 460-473. Edinburgh: Institution of Civil Engineers. Thomas Telford Ltd. https://doi.org/10.1680/cmsb.41318.0044.

van der Meer, J., B. Hardeman, G. J. Steendam, H. Schüttrumpf, and H. Verheij. 2010. “Flow depths and velocities at crest and landward slope of a dike, in theory and with the wave overtopping simulator”. In *Proc. Coastal Eng.* 1 (32): 10. https://doi.org/10.9753/icce.v32.structures.10.

van der Meer, J., A. van Hoven, M. Paulissen, G. J. Steendam, H. J. Verheij, G. Hoffmans, and G. Kruse. 2015. Handreiking Dijkbekledingen Deel 5: Grasbekledingen. https://tl.iplo.nl/zoeken/@193681/uittrekmechanisme-faalmechanismen-grasbekleding/.

van der Meer, J., N. W. H. Allsop, T. Bruce, J. De Rouck, A. Kortenhaus, T. Pullen, H. Schüttrumpf, P. Troch, and B. Zanuttigh. 2018. “Eurotop: Manual on wave overtopping of sea defences and related structures: an overtopping manual largely based on European research, but for world-wide application." Technical Report. www.overtopping-manual.com.

Westoby, M. J., J. Brasington, N. F. Glasser, M. J. Hambrey, and J. M. Reynolds. 2012. 'Structure-from-motion photogrammetry: A low-cost, effective tool for geoscience applications. *Geomorphology*., 179: 300-314. https://doi.org/10.1016/j.geomorph.2012.08.021.

Zhang, C., A. Sun, M.A. Hassan, and C. Qin. 2022. "Assessing through-water structure-from-motion photogrammetry in gravel-bed rivers under controlled conditions". *Remote Sens*., 14 (21): 5351. https://doi.org/10.3390/rs14215351.

List of figures captions

Fig. 1. Aerial view of Polder2C's project site, LLHPP, and locations for bare-clay (BC) and lime-treated clay (LTC) experiments.

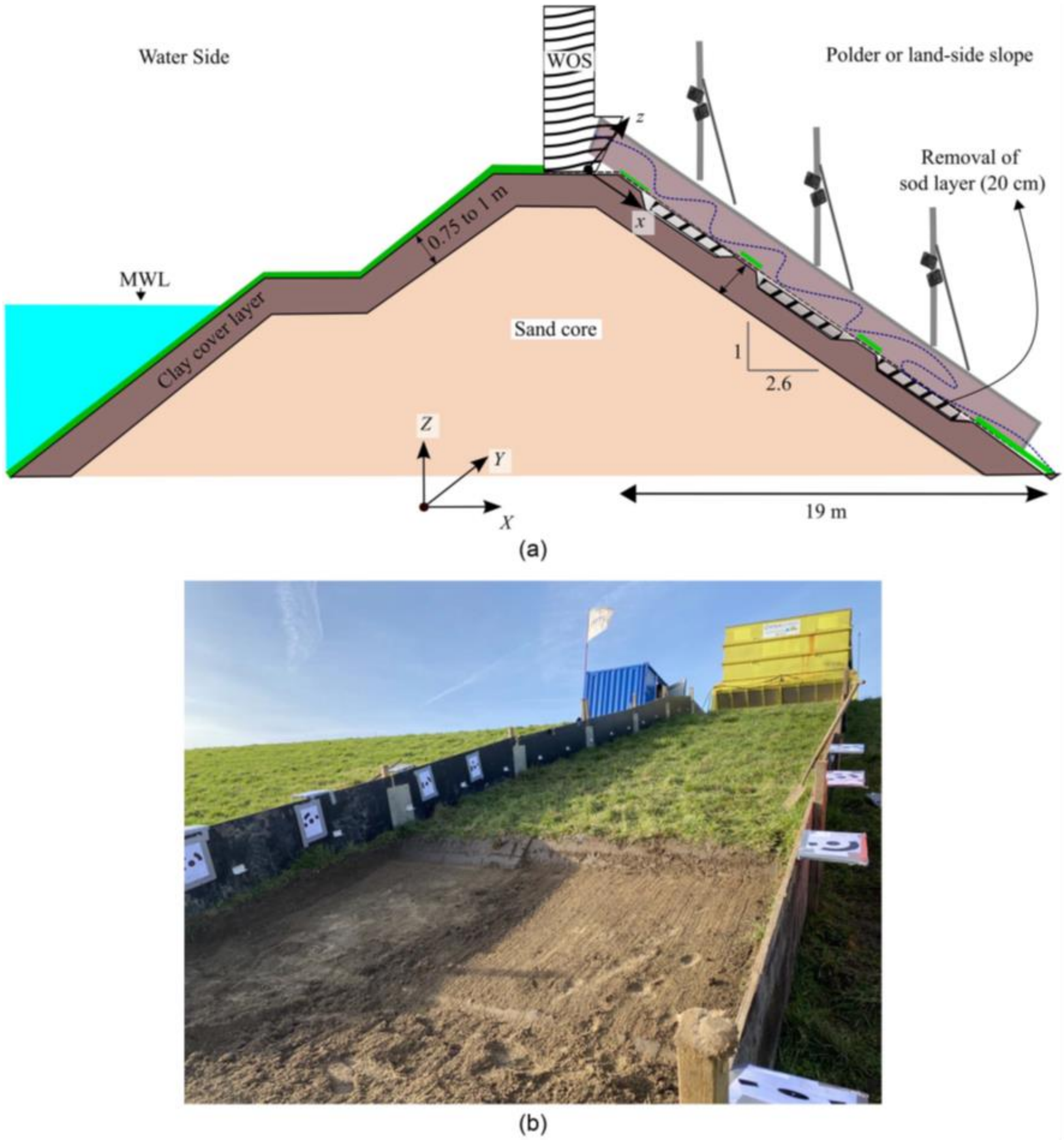

Fig. 2. (a) schematic view of typical Dutch levee cross-section as well as BC test layout, and (b) example of prepared testing section for BC experiments.

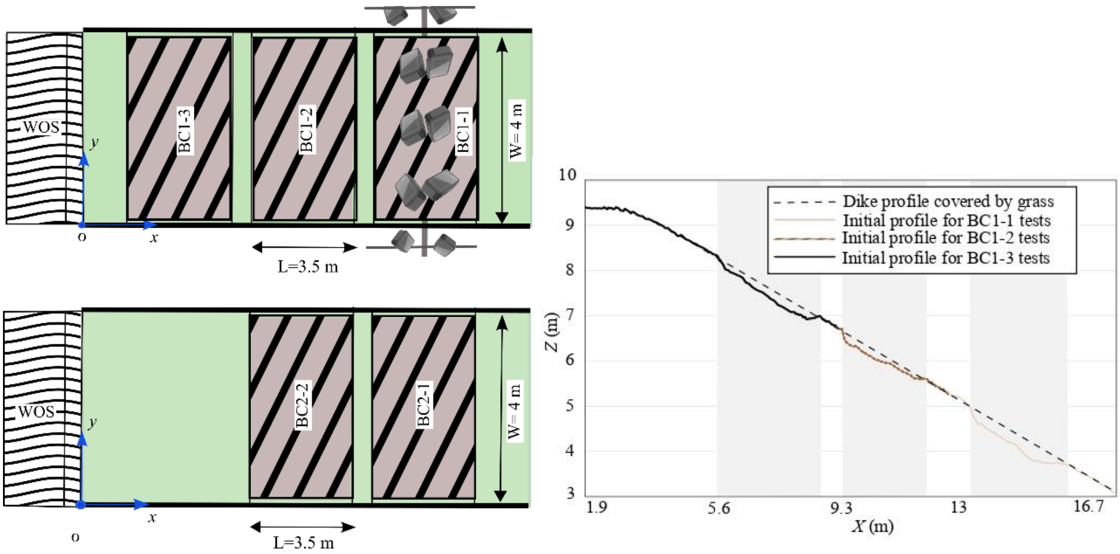

(a) (b)

Fig. 3. (a) BC test flumes and section layouts; and (b) initial and excavated levee slope profiles for all BC1 sections (obtained from photogrammetry).

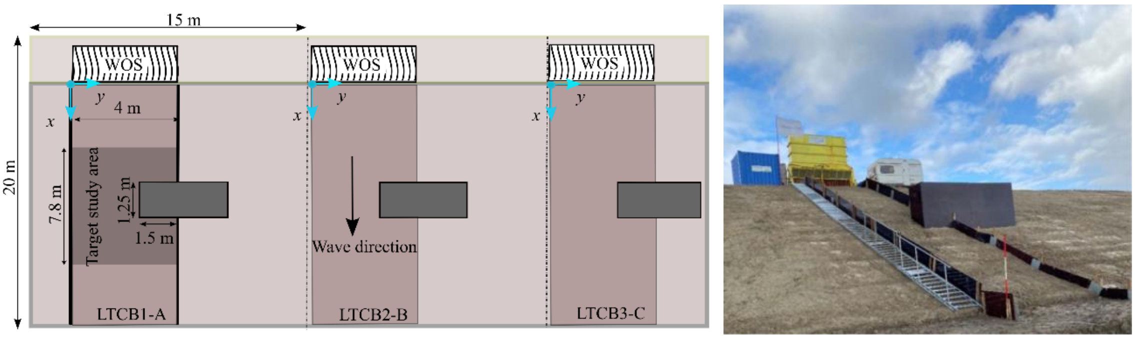

(a) (b)

Fig. 4. (a) LTCB test location including layout of all sections and target study area; and (b) constructed section.

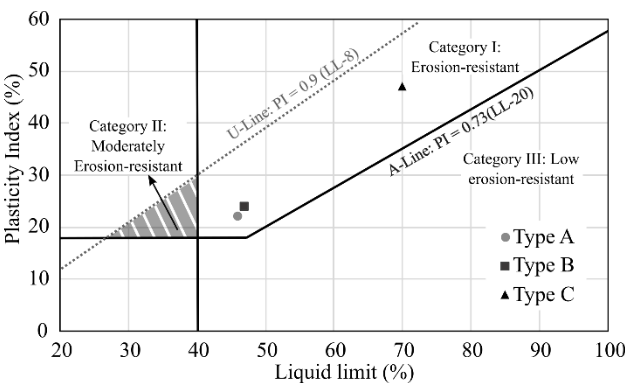

Fig. 5. Clay soil classification for Polder2Cs levee revetment according to Dutch dike regulations.

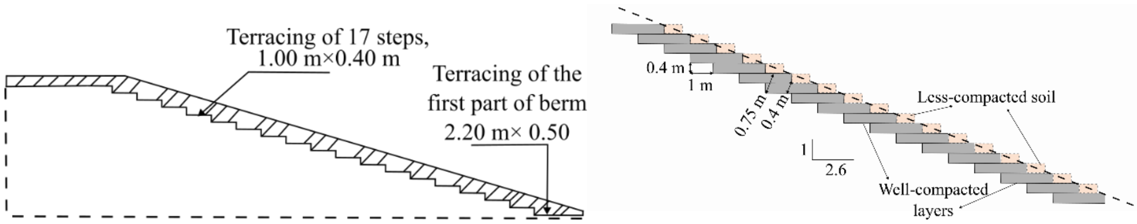

(a) (b)

Fig. 6. (a) Removal of levee's old cover layer and (b) construction of new lime-treated clays cover layer.

(a) (b)

Fig. 7. Wave overtopping simulator (WOS) located on levee crest, (a) the gate or opening valve and (b) an example of releasing wave.

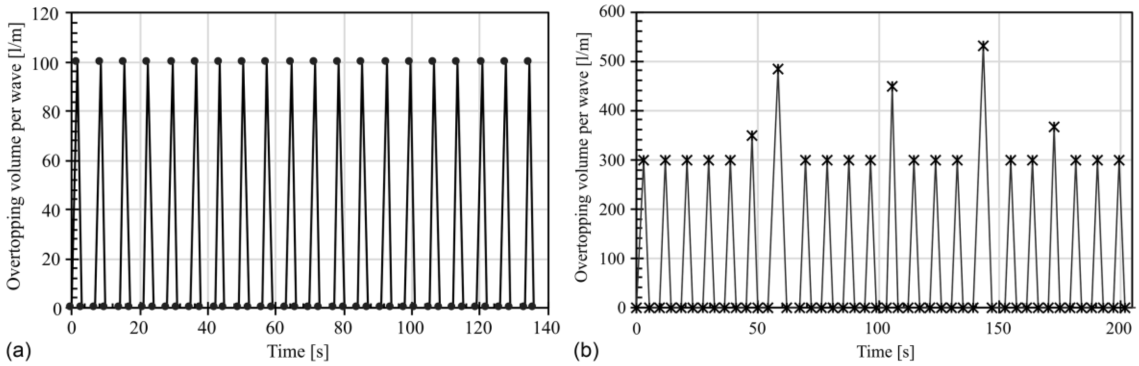

Fig. 8. Examples of distributions for (a) irregular waves, and (b) regular waves patterns (clusters of 20 waves with different volumes).

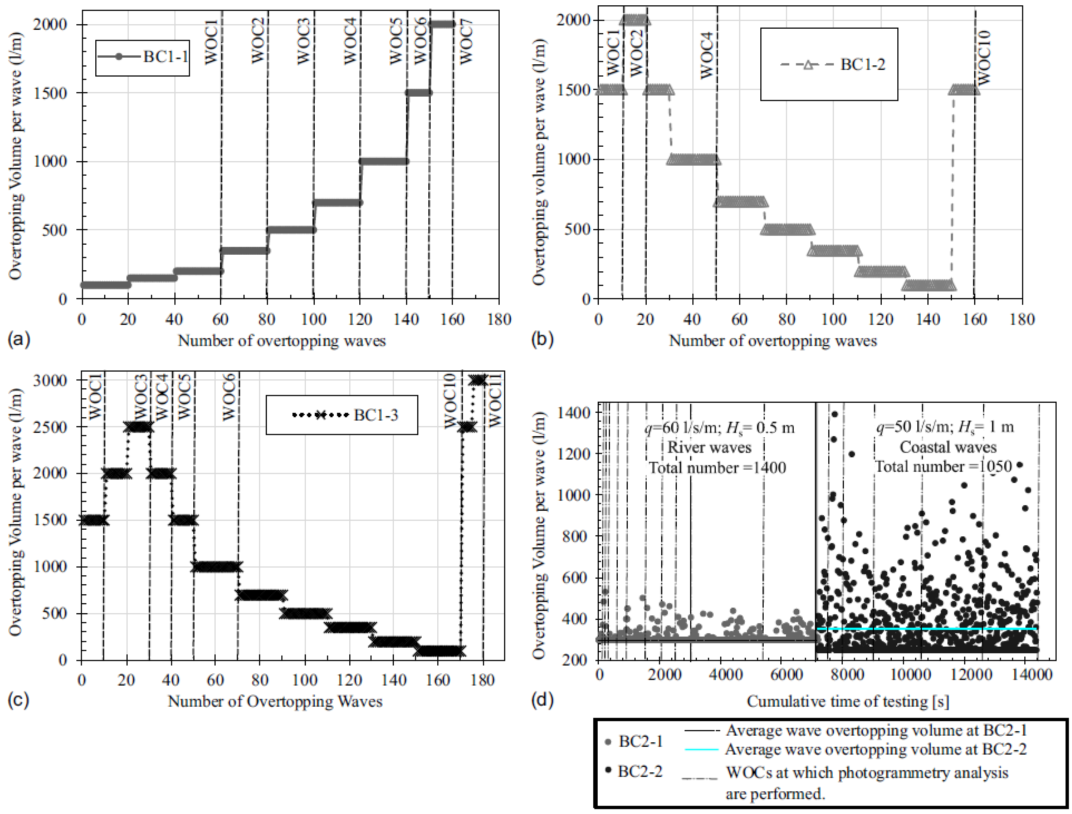

Fig. 9. Regular waves with arbitrary patterns released during BC1 experiments at (a) BC1-1, (b) BC1-2 and (c) BC1-3 sections; (d) Irregular waves released during BC2 experiments.

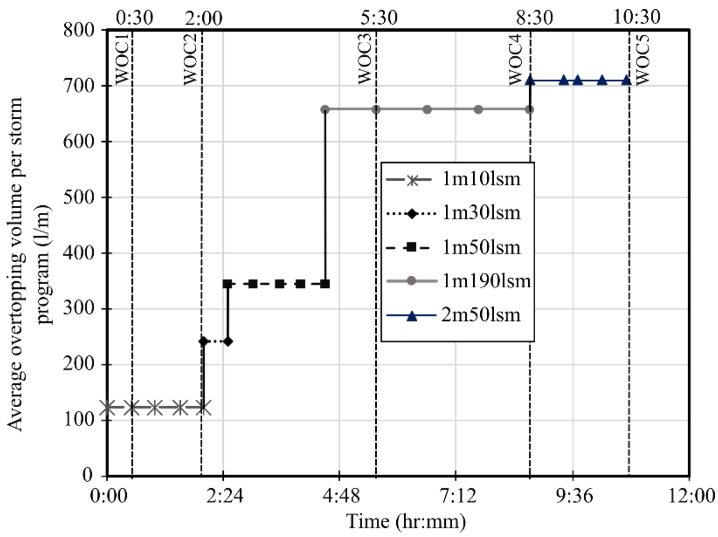

Fig. 10. Wave overtopping storm programs tested at LTCB sections.

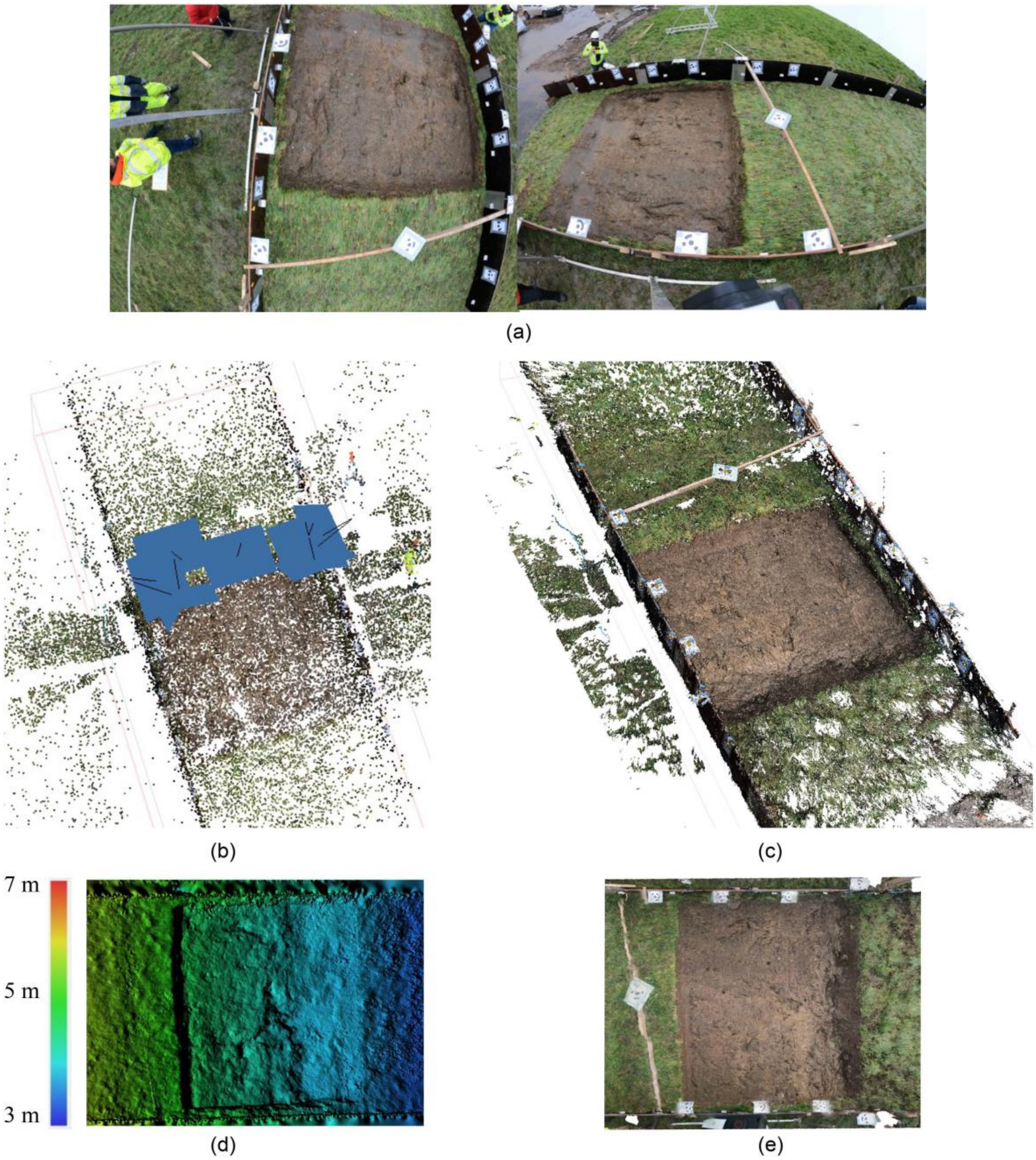

Fig. 11. Photogrammetry processing: (a) Importing raw photos, (b) Aligning Photos, Generating (c) Dense Point Cloud, (d) Digital Elevation Model (DEM), and (e) Orthophoto.

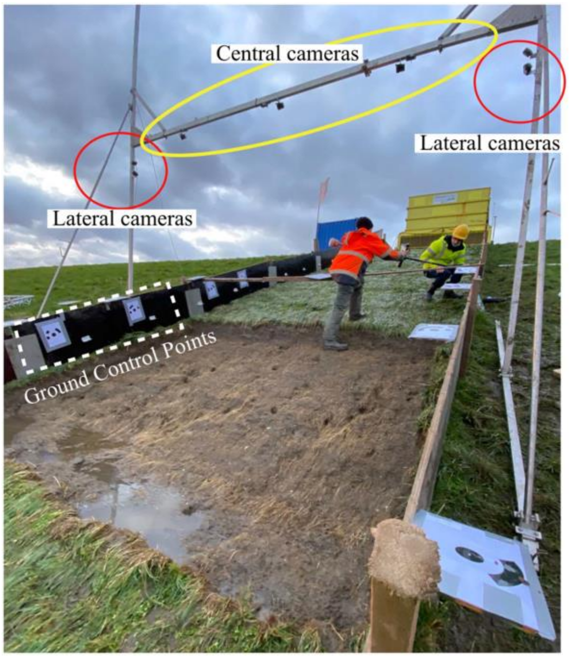

Fig. 12. Multiple fixed camera set-up.

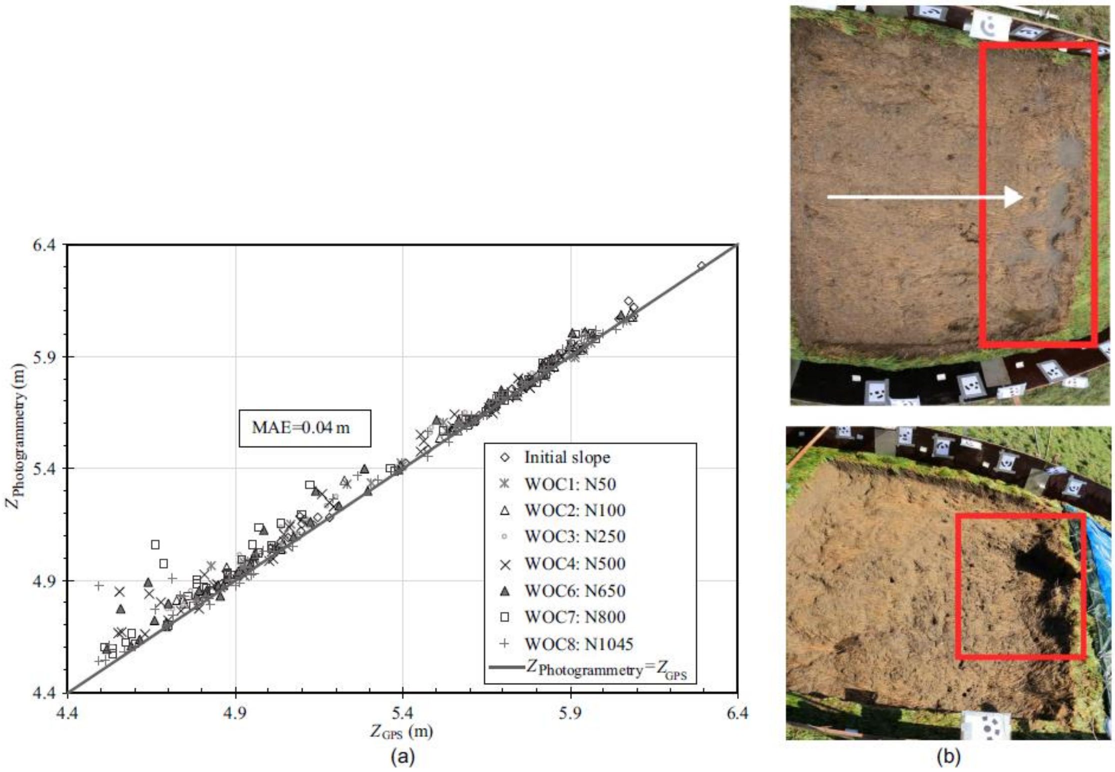

Fig. 13. (a) Photogrammetric verification versus RTK measurements for multicamera set-up at section BC2-2; (b) water-shadow negative effects.

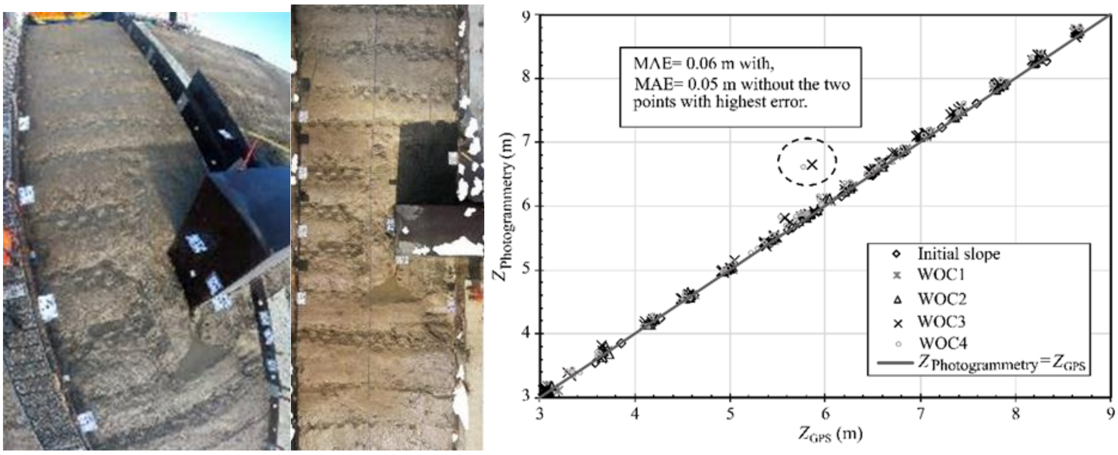

(a) (b) (c)

Fig. 14. (a) LTCB1-A final state highlighting the adverse effect of water, (b) corresponding orthophoto (b), and (c) Photogrammetric verification versus RTK measurements for one mobile camera at this section.

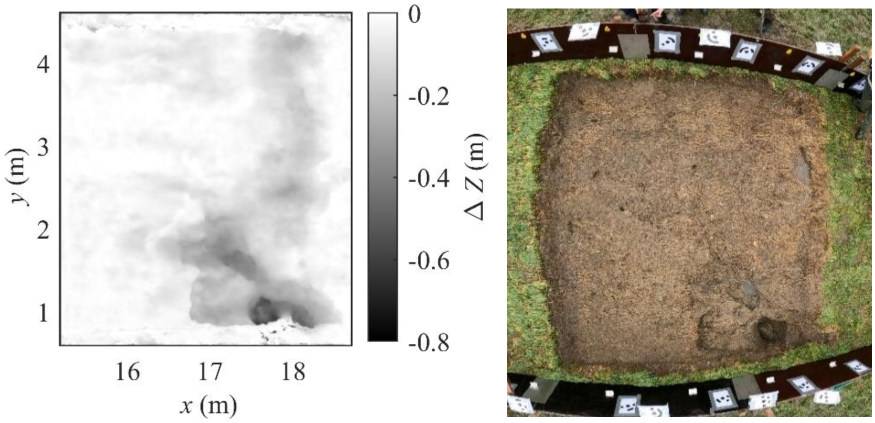

(a)

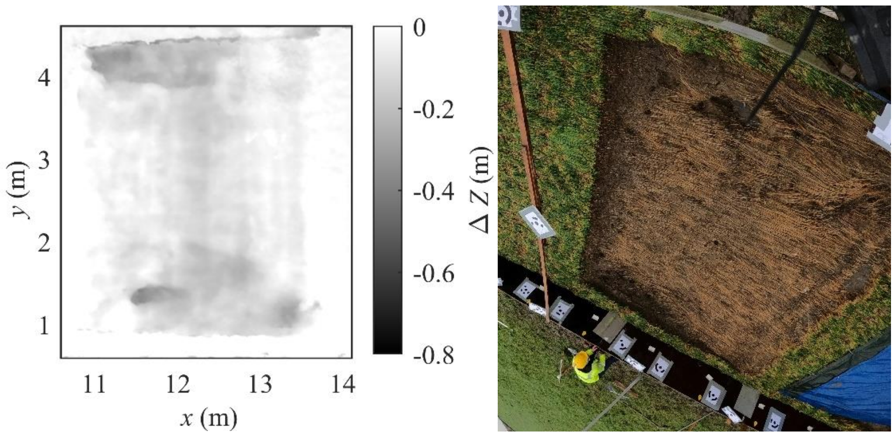

(b)

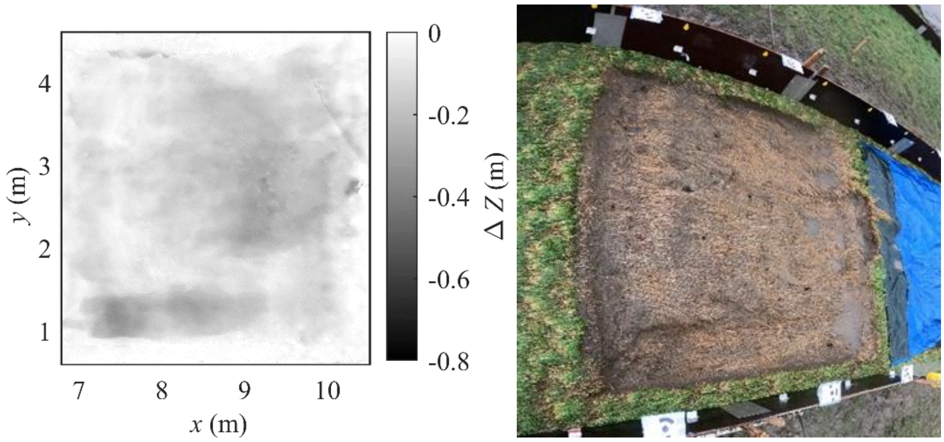

(c)

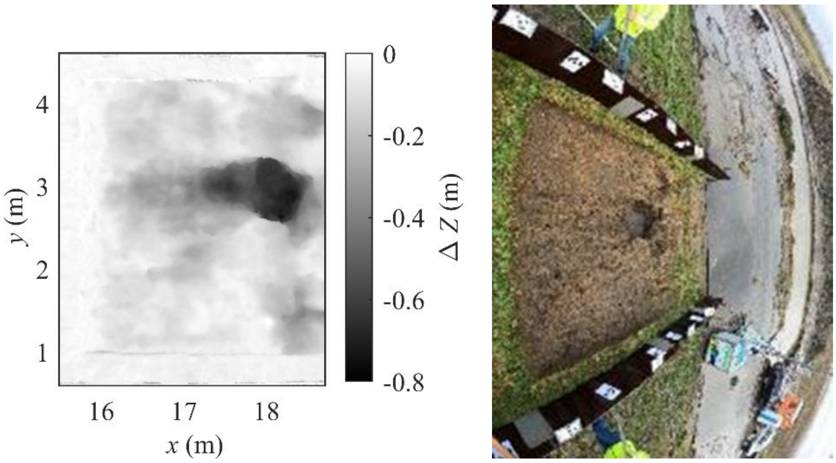

(d)

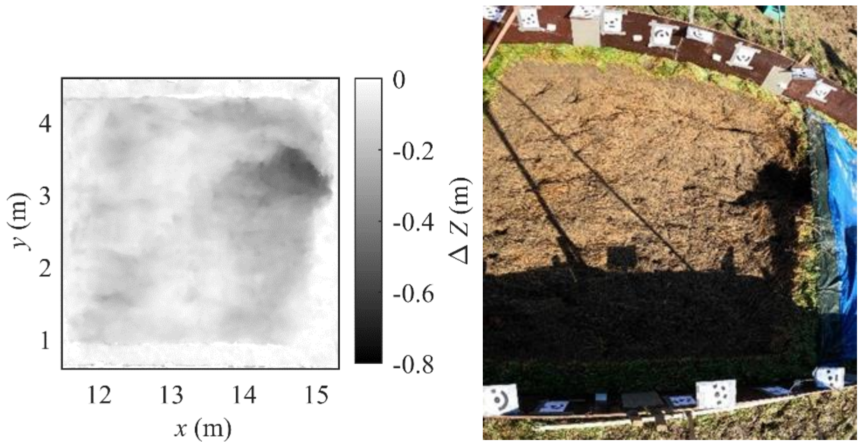

(e)

Fig. 15. Total erosion depth at test sections (a) BC1-1, (b) BC1-2, (c) BC1-3, (d) BC2-1 and (e) BC2-2 and corresponding GoPro photos. Flow direction is from left to right.

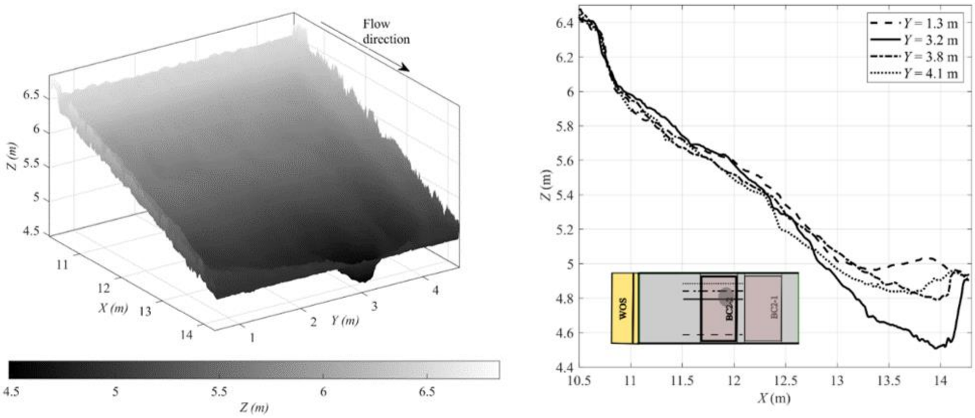

(a) (b)

Fig. 16. (a) 3D view of BC2-2, and (b) longitudinal bed level profiles at different transversal distances.

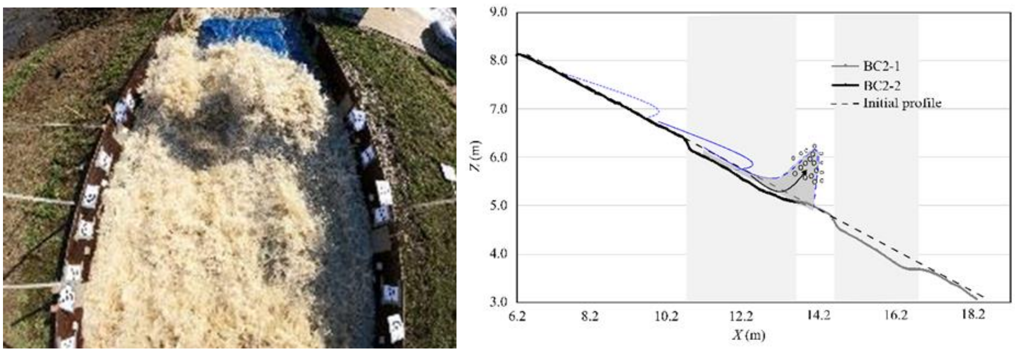

Fig. 17. Large wave break and jump at section (a) BC2-2, and (b) schematic illustration of the trajectory of an overtopping wave.

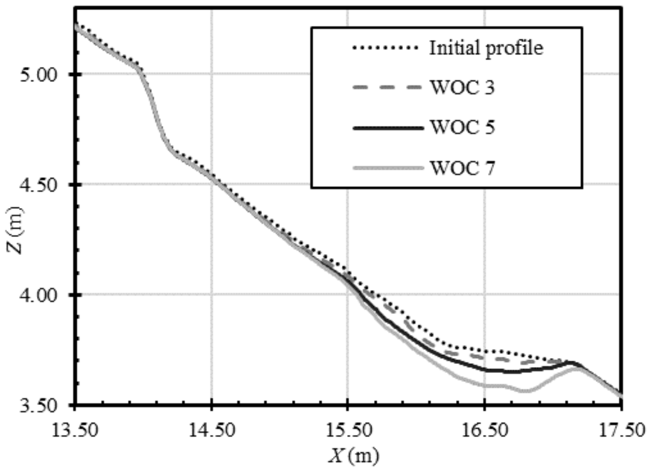

Fig. 18. Average longitudinal bed profiles at BC1-1.

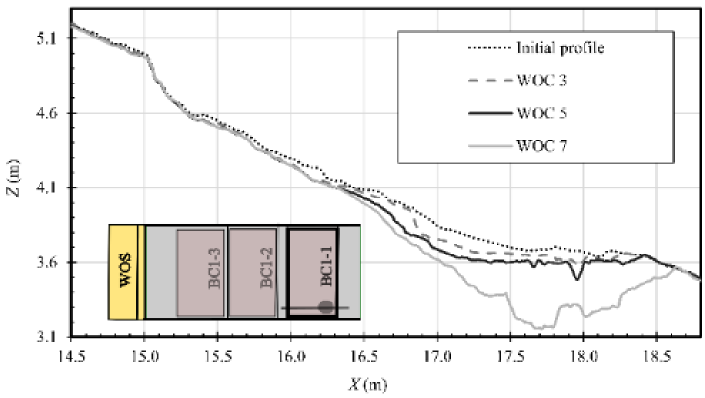

(a)

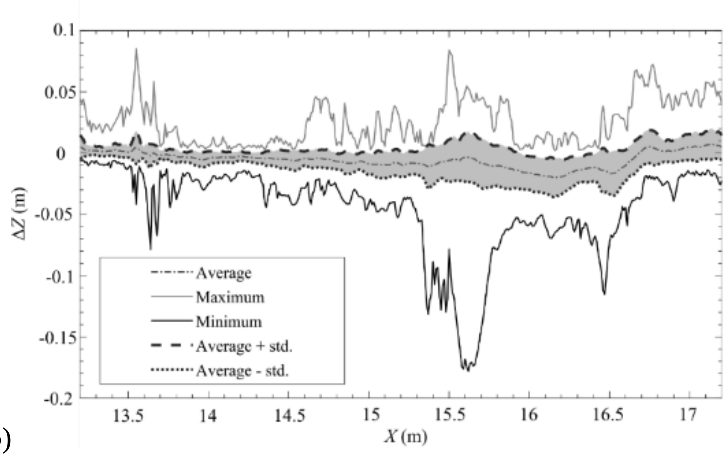

(b)

Fig. 19. (a) Maximum bed level changes at BC1-1, and (b) bed level irregularity across BC1-1 at WOC3.

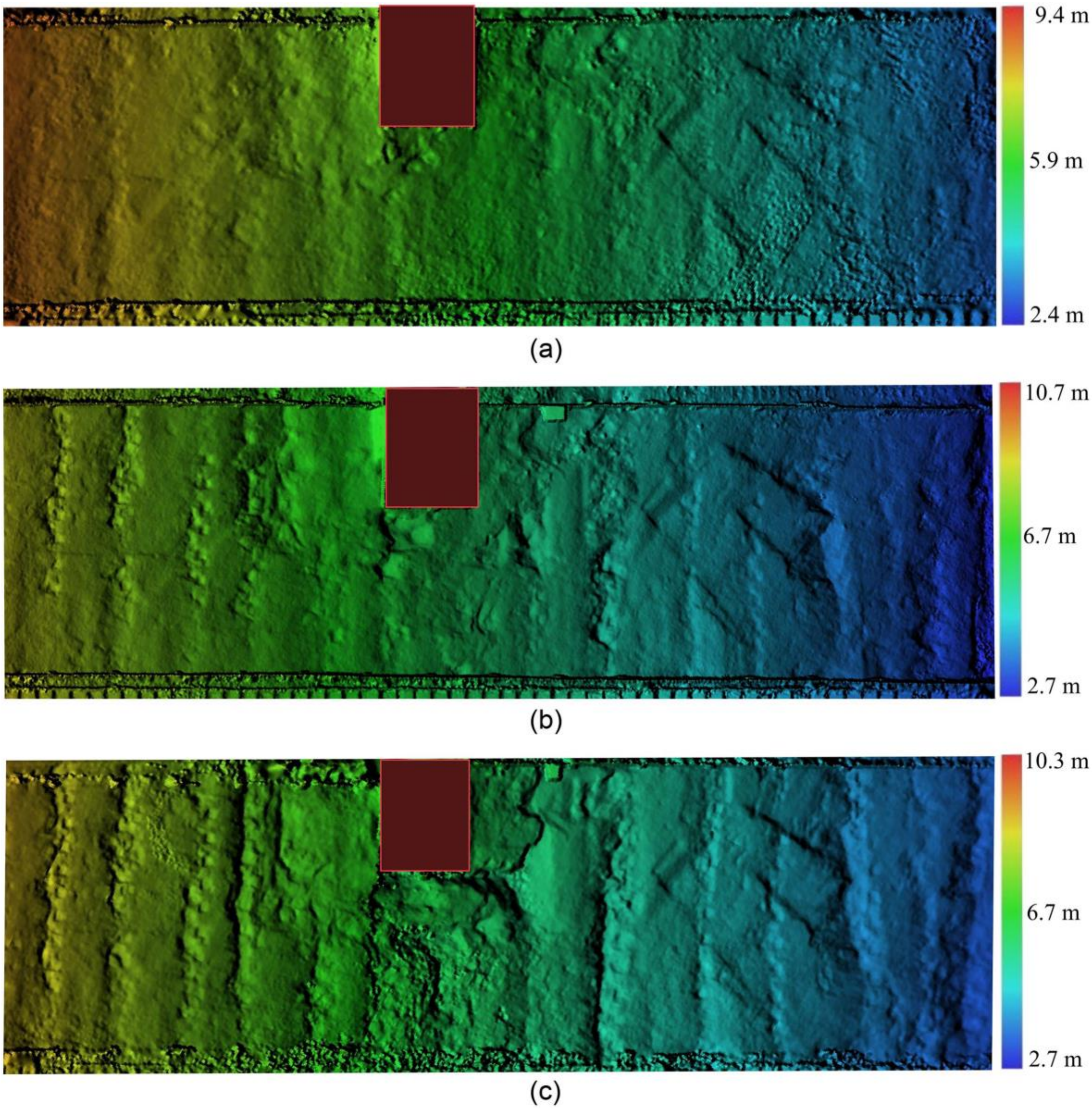

Fig. 20. Levee slope evolution during wave overtopping experiments at LTCB1-A: for (a) Initial state; (b) WOC1, and (c) WOC4 (flow direction left to right).

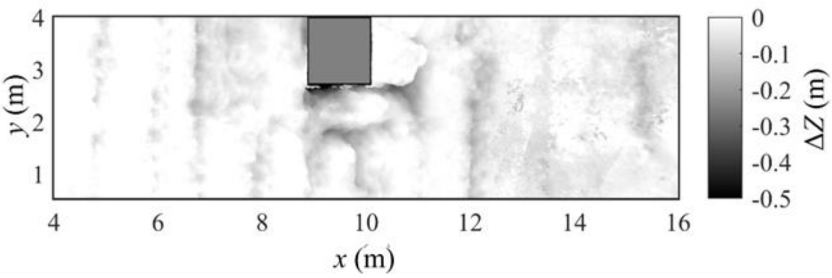

(a)

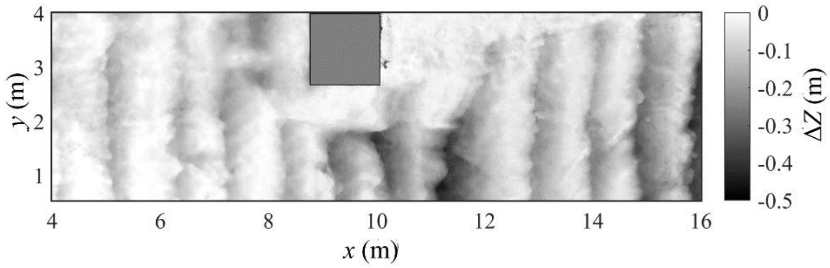

(b)

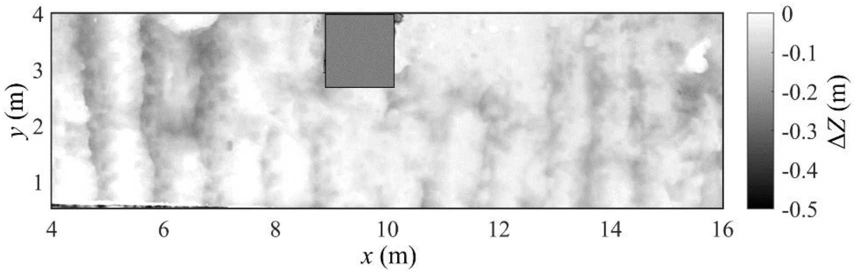

(c)

Fig. 21. Overall soil erosion in *xy* plane: (a) LTCB1-A; (b) LTCB2-B; and (c) LTCB3-C.

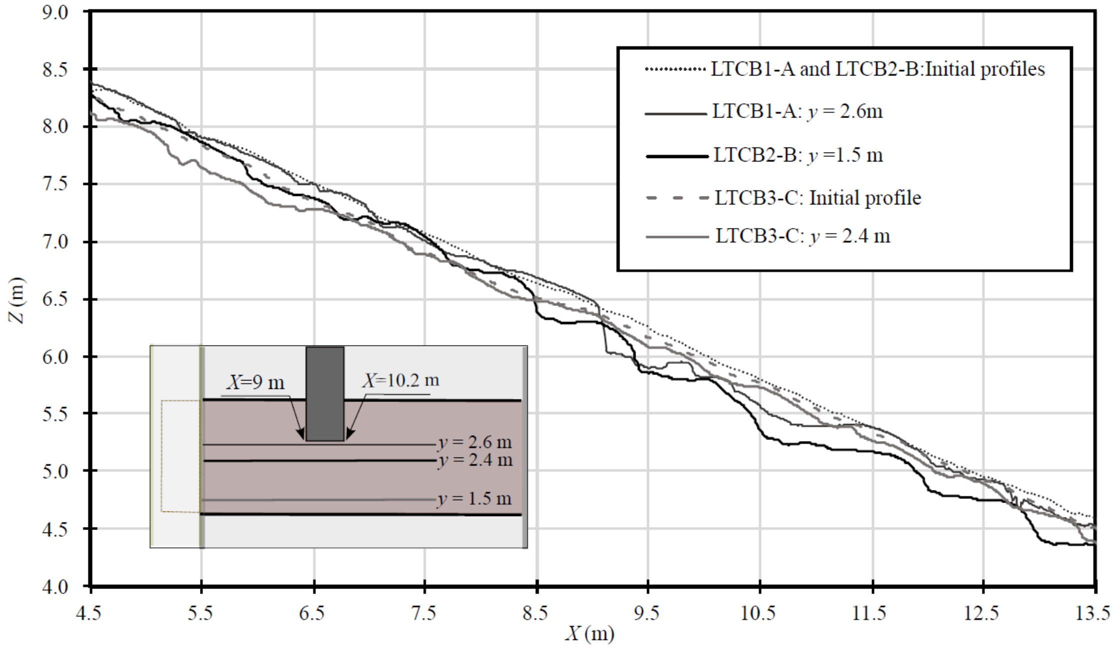

Fig. 22. Initial, and final bed level profiles of maximum erosion depth for WOC4.

Table 1. Irregular wave overtopping programs.

Test name	Wave pattern acronym	Height H_s (m)	Discharge q ($m^3/s/m$)	probability of overtopping per wave	Total Wave numbers
BC2-1	0.5m60lsm	0.5	0.060	0.992	1419
BC2-2	1m50lsm	1	0.050	0.725	1045
LTCB1-A, LTCB2-B and LTCB3-C	1m10lsm	1	0.010	0.340	585
LTCB1-A, LTCB2-B and LTCB3-C	1m30lsm*	1	0.030	0.590	222
LTCB1-A, LTCB2-B and LTCB3-C	1m50lsm	1	0.05	0.725	1045
LTCB1-A, LTCB2-B and LTCB3-C	1m190lsm*	1	0.190	1.000	1991
LTCB2-B and LTCB3-C	2m50lsm	2	0.050	0.435	510

*Except 1m30lsm and 1m190lsm which lasted respectively 30 minutes and 4 hours all other wave programs simulate 2-hour storm events.

Table 2. Summary of all erosion tests and photo acquisition method.

Test name	Test monitoring type	Location on slope	Overtopping wave type	Duration (hr:mm)
Bare-clay 1				
BC1-1	Multicamera on fixed frame	Lower	Regular waves	0:35
BC1-2	Multicamera on fixed frame	Middle	Regular waves	0:45
BC1-3	Multicamera on fixed frame	Upper	Regular waves	1:00
Bare-clay 2				
BC2-1	Multicamera on fixed frame	Lower	Irregular waves	2:00
BC2-2	Multicamera on fixed frame	Middle	Irregular waves	2:00
Lime-treated clay				
LTCB1-A	One mobile camera	Entire	Irregular waves – with building	8:45
LTCB2-B	One mobile camera	Entire	Irregular waves – with building	10:45
LTCB3-C	One mobile camera	Entire	Irregular waves – with building	10:45

Table 3. Agisoft Metashape processing parameters and output model characteristics.

Operation	Parameters	Multicamera	Mobile camera
Photo selection	No. of photos	10	80
Camera calibration	Camera type	Fisheye	Fisheye
Detect markers	GCP detection	Automatic	Automatic and manual
Align photos	Key point limit	10×10^4	4×10^4
	Tie point limit	5×10^4	4×10^3
	Accuracy	Highest	Highest
	Sparse points	7.5×10^4	7×10^4
Build Dense Cloud	Quality	High	High
	Dense points	10×10^6	30×10^6
	Total Error* (m)	1.7×10^{-2}	2.7×10^{-2}
Build DEM	Resolution (m)	2.62×10^{-3}	2.9×10^{-3}

* Total error is calculated as root mean square errors (distance between input and estimated coordinates) of all GCPs.

Table 4. Moments for which photogrammetry processing were performed at BC1 and BC2 sections.

Section	Waves condition	WOC1	WOC2	WOC3	WOC4	WOC5	WOC6	WOC7	WOC8	WOC9	WOC10	WOC11
BC1												
BC1-1	*Vol* [l/m] N	200 60	350 80	500 100	700 120	1000 140	1500 150	2000 160	-	-	-	-
BC1-2	*Vol* [l/m] N	1500 10	2000 20	-	1000 50	-	-	-	-	-	1500 160	-
BC1-3	*Vol* [l/m] N	1500 10	-	2500 30	2000 40	1500 50	1000 70	-	-	-	100 174	3000 184
BC2												
BC2-1	N	20	40	60	120	180	300	400	500	600	1050	1419
BC2-2	N	50	100	250	500	650	800	1045	-	-	-	-

Table 5. Overall performance of BC and LTCB under wave overtopping tests.

Test name	Test duration (hr:mm)	Average wave overtopping volume per storm event (l/m)	Total wave overtopping volume (m^3)	Total area (m^2)	Total erosion volume (m^3)	Average erosion depth (cm)	Maximum erosion depth (cm)
BC1-1	0:35	590	380	13.0	0.95	7.36	64
BC1-2	0:45	760	488	10.8	0.79	7.34	36
BC1-3	1:00	980	721	12.6	1.52	12.04	34
BC2-1	2:00	305	1730	9.9	1.62	16.34	75
BC2-2	2:00	345	1440	12.92	1.32	10.2	55
LTCB1-A	8:45	123-242-345-658	7416	26	0.85	3.26	54
LTCB2-B	8:45	123-242-345-658	7416	26	2.56	10.09	45
LTCB3-C	8:45	123-242-345-658	7416	26	1.59	6.16	26